New Journal of Physics
The open access journal at the forefront of physics

Deutsche Physikalische Gesellschaft DPG IOP Institute of Physics

PAPER • OPEN ACCESS

Bi ultra-thin crystalline films on InAs(1 1 1)A and B substrates: a combined core-level and valence-band angle-resolved and dichroic photoemission study

To cite this article: L Nicolaï *et al* 2019 *New J. Phys.* **21** 123012

View the article online for updates and enhancements.

This content was downloaded from IP address 88.133.233.228 on 03/03/2020 at 13:14

New Journal of Physics
The open access journal at the forefront of physics

Deutsche Physikalische Gesellschaft DPG
IOP Institute of Physics

Published in partnership with: Deutsche Physikalische Gesellschaft and the Institute of Physics

OPEN ACCESS

RECEIVED
25 July 2019

REVISED
26 October 2019

ACCEPTED FOR PUBLICATION
21 November 2019

PUBLISHED
12 December 2019

Original content from this work may be used under the terms of the Creative Commons Attribution 3.0 licence.

Any further distribution of this work must maintain attribution to the author(s) and the title of the work, journal citation and DOI.

PAPER

Bi ultra-thin crystalline films on InAs(1 1 1)A and B substrates: a combined core-level and valence-band angle-resolved and dichroic photoemission study

L Nicolaï[1], J-M Mariot[2,3], U Djukic[4], W Wang[5], O Heckmann[4,6], M C Richter[4,6], J Kanski[7], M Leandersson[5], T Balasubramanian[5], J Sadowski[8,9,10], J Braun[11], H Ebert[11], I Vobornik[12], J Fujii[12], J Minár[1] and K Hricovini[4,6]

[1] New Technologies–Research Centre, University of West Bohemia, Univerzitní 8, 306 14 Pilsen, Czech Republic
[2] Sorbonne Université, CNRS (UMR 7614), Laboratoire de Chimie Physique–Matière et Rayonnement, 4 place Jussieu, F-75252, Paris Cedex 05, France
[3] Synchrotron SOLEIL, L'Orme des Merisiers, Saint-Aubin, BP 48, F-91192, Gif-sur-Yvette, France
[4] Laboratoire de Physique des Matériaux et des Surfaces, Université de Cergy-Pontoise, 5 mail Gay-Lussac, F-95031, Cergy-Pontoise, France
[5] MAX IV Laboratory, Lund University, PO Box 118, SE-221 00, Lund, Sweden
[6] LIDYL, CEA, CNRS (UMR 9222), Université Paris-Saclay, CEA Saclay, F-91191, Gif-sur-Yvette Cedex, France
[7] Chalmers University of Technology, Department of Physics, SE-412 96, Gothenburg, Sweden
[8] Department of Physics and Electrical Engineering, Linnaeus University, SE-391 82, Kalmar, Sweden
[9] Institute of Physics, Polish Academy of Sciences, al. Lotników 32/46, 02-668 Warsaw, Poland
[10] Faculty of Physics, University of Warsaw, ul. Pasteura, 02-0933 Warsaw, Poland
[11] Ludwig-Maximilians-Universität München, Department Chemie, Butenandtstraße 11, D-81377, München, Germany
[12] Istituto Officina dei Materiali, TASC Laboratory, CNR, Area Science Park–Basovizza, Strada Statale 14, km 163.5, I-34149, Trieste, Italy

E-mail: karol.hricovini@u-cergy.fr

Keywords: bismuth, indium arsenide, growth, ultra-thin films, angle-resolved photoemission, electronic structure calculations, circular dichroism

Abstract

The growth of Bi on both the In-terminated (A) face and the As-terminated (B) face of InAs(1 1 1) has been investigated by low-energy electron diffraction, scanning tunnelling microscopy, and photoelectron spectroscopy using synchrotron radiation. The changes upon Bi deposition of the In 4*d* and Bi $5d_{5/2}$ photoelectron signals allow to get a comprehensive picture of the Bi/InAs(1 1 1) interface. From the early stage the Bi growth on the A face is epitaxial, contrary to that on the B face that proceeds via the formation of islands. Angle-resolved photoelectron spectra show that the electronic structure of a Bi deposit of ≈10 bi-layers on the A face is identical to that of bulk Bi, while more than ≈30 bi-layers are needed for the B face. Both bulk and surface electronic states observed are well accounted for by fully relativistic *ab initio* calculations performed using the one-step model of photoemission. These calculations are used to analyse the dichroic photoemission data recorded in the vicinity of the Fermi level around the $\overline{\Gamma}$ point of the Brillouin zone.

1. Introduction

The discovery a decade ago of the family of topological insulators [1–4] has brought to the front a new and fascinating area of physics. The simplicity of the topological insulator surface states, the robustness of both topological properties and surface metallicity under external perturbations, and the prediction of novel quantized states arising from the peculiar coupling between magnetic and electric fields make these systems of great interest for developing the next generation of electronic and spintronic devices.

Focusing on the spintronics aspect, one of the possibilities to obtain spin-polarized electronic currents is to use the spin splitting in momentum space of surface states that results from the breaking of inversion symmetry at a surface (Rashba effect) [5]. This has recently stimulated studies of the electronic structure of Bi and Bi-based

© 2019 The Author(s). Published by IOP Publishing Ltd on behalf of the Institute of Physics and Deutsche Physikalische Gesellschaft

compounds, because of the large spin–orbit interaction in this heavy group-V element (see, e.g. [6]). Along this line many investigations of the changes with respect to bulk Bi of the electronic structure of Bi thin films deposited on semiconductors, e.g. Si(1 1 1) [7, 8], SiC(0 0 0 1) [9], and highly-oriented pyrolytic graphite [10], have been performed. Such studies on Bi thin films are also of importance for a better understanding of the physical properties of topological insulators [1, 3, 11–13] (see also [14] review).

As far as thin layers are concerned, it has been theoretically predicted from first-principles calculations that two-dimensional bismuth could behave as a topological insulator [15–18]. These studies reveal that key factors leading to the appearance of a topological behaviour are tensile strain due to the lattice mismatch at the Bi/substrate interface and formation of chemical bonds at the interface. In particular it has been established that bismuthene grown on a SiC(0 0 0 1) substrate is nontrivial [19]. Along these lines, Reis *et al* [20] have shown in a combined theoretical and experimental study that in this case it is possible to obtain a quasi two-dimensional topological insulator where both a large gap and a strong spin–orbit coupling are present. Thus studying Bi/substrate interfaces can be expected to reveal new physical properties and provide improved means to engineer them. On the experimental side, III–V semiconductor substrates have not been explored up to now. We report here on a study of the electronic structure of Bi films deposited on both A (In-terminated) and B (As-terminated) faces of InAs(1 1 1). Although some results on the growth of Bi on InAs(1 1 1)B have been reported in the past [21], the Bi/InAs(1 1 1)A interface has not yet been investigated to our knowledge.

We have followed the structural and electronic changes that occur during the deposition of Bi on both A and B faces of InAs(1 1 1) by means of low-energy electron diffraction (LEED), scanning tunnelling microscopy (STM), and core-level as well as valence-band photoelectron spectroscopy (PES) using synchrotron radiation. The growth mode is found to be dependent on the substrate side. An epitaxial growth is evidenced on the A side and, as a consequence, ultra-thin Bi films deposited on InAs(1 1 1)A have an electronic structure showing all the characteristics of bulk Bi. On the contrary the Bi growth on the B face proceeds via the formation of islands. The angle-resolved PES (ARPES) data on Bi/InAs(1 1 1)A are well accounted for by *ab initio* fully relativistic one-step photoemission model calculations performed in the framework of the density functional theory combined with the multiple scattering formalism. The confrontation between experimental data and theoretical simulations helps to identify the nature of the electronic states close to the Fermi level.

2. Experimental and computational methods

The experiments were performed at the APE beamline [22] of the Elettra synchrotron radiation facility (Trieste, Italy) and at the I3 beamline [23] of the MAX III synchrotron (MAX-lab, Lund, Sweden). The substrates were cut from 0.5 mm thick *n*-doped (3×10^{18} cm^{-3}) InAs(1 1 1) wafers (Wafer Technology Ltd., UK) polished on both sides. After degassing, both InAs(1 1 1)A and B surfaces were prepared (simultaneously) by repeated cycles of ion bombardment (Ar^+, 600 eV) and annealing at 400 °C until a sharp (2×2) or (1×1) LEED pattern for side A or side B, respectively, was obtained (see, e.g. [24] and the references cited therein). Bismuth was deposited from a Knudsen cell at a rate of about 0.5 bi-layer (BL) min^{-1}, under a pressure lower than 4×10^{-10} Torr, on substrates at room temperature.

The band structure calculations were performed using the SPR-KKR package [25] that is based on the Korringa–Kohn–Rostoker method, which uses the Green's function formalism within the multiple scattering theory and the Dirac equation, thus fundamentally containing all relativistic effects, such as spin–orbit coupling. The bulk potential that was used as an input to simulate the ARPES spectra within the one-step model of photoemission [26, 27] results from calculations performed within the local density and atomic sphere approximations. The model of Rundgren–Malmström [28] was used to describe the crystal potential in the surface region. The relaxation of the surface was taken into account using the structural data given in [29]. For the bulk, the lattice parameters in the hexagonal description ($a = 4.5332$ and $c = 11.7967$ Å) were used [6].

3. Results and discussion

3.1. Pristine InAs(1 1 1) surfaces

While a (2×2) LEED pattern is observed for InAs(1 1 1)A (figure 1(a)), the InAs(1 1 1)B surface is unreconstructed (not shown); this is due to charge transfer between the outermost layers [30]—which also explains the ≈250 meV shift towards the high binding energy (BE) side of the main peak of the In 4*d* PES spectrum for the A side with respect to the B side—and/or the presence of In vacancies on the In-terminated A surface (see [31–33], and the references therein). The In 4*d* PES spectra for both the A side and the B side of InAs(1 1 1) are in agreement with those reported previously [21, 34, 35]. They are given in figure 2 to help comparison with those of the Bi-covered substrates in the following discussion.

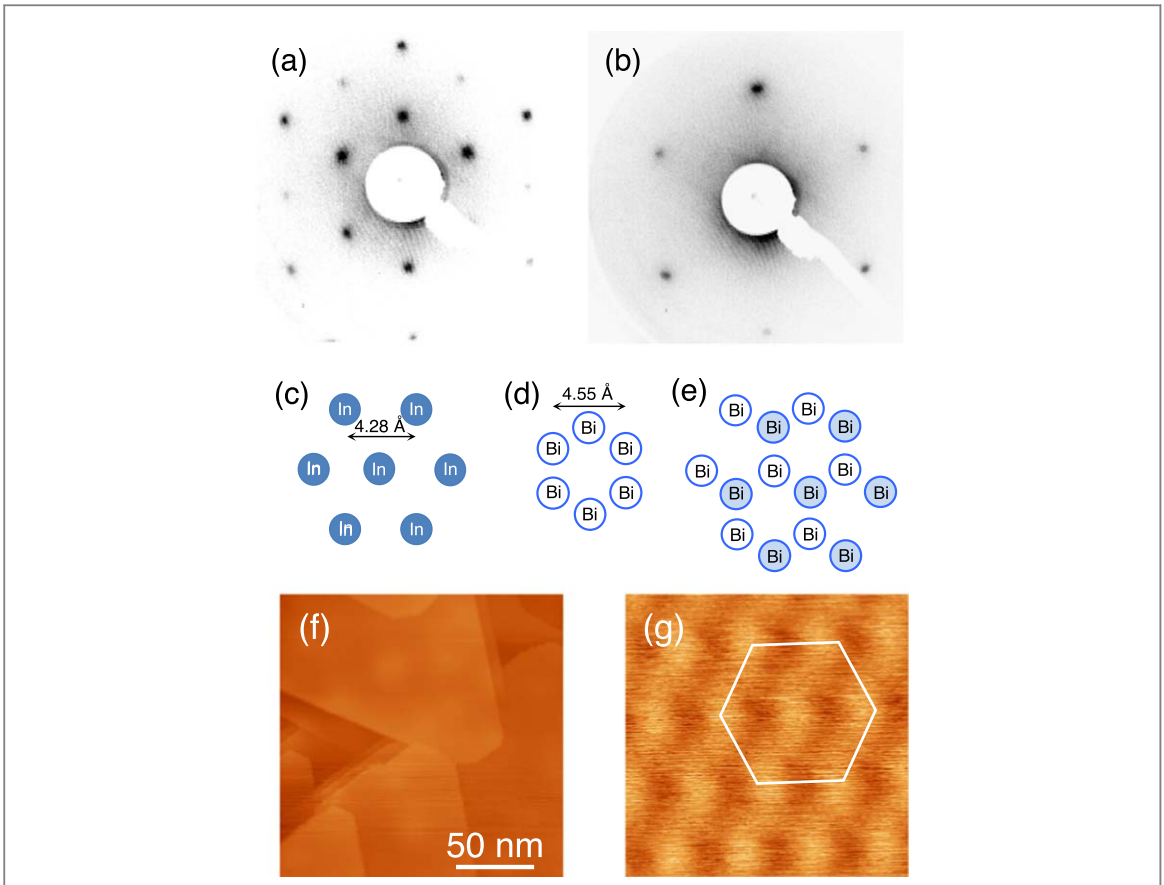

Figure 1. (a) and (b) LEED patterns of pristine InAs(1 1 1)A showing the (2 × 2) reconstruction (taken at 52 eV) and of a 10 BL Bi deposit on InAs(1 1 1)A (taken at 22 eV). Schematic arrangement of atoms (top view) in: (c) the top layer of InAs(1 1 1)A (In-terminated) and (d) the first BL of Bi(1 1 1). (e) A possible arrangement of the Bi deposit on InAs(1 1 1)A (the Bi atoms located above the In atoms of the substrate are in light blue). (f) and (g) STM images of the InAs(1 1 1)A substrate covered by 10 BL Bi. The hexagon in (g) is a guide to the eye showing the arrangement of the Bi atoms.

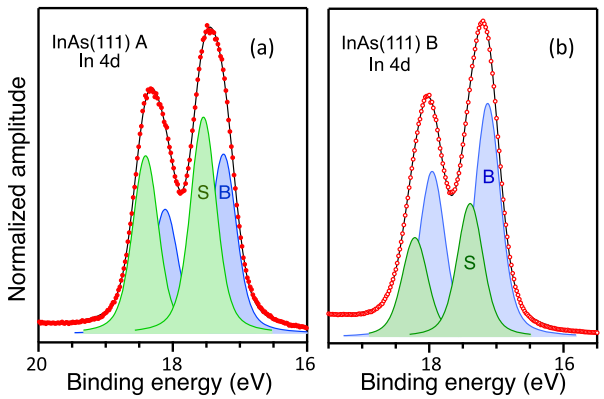

Figure 2. In 4*d* PES spectra of clean InAs(1 1 1): (a) A side; (b) B side. Raw data are shown as dots; the lines are the fit to the data and the components (denoted by B for the bulk and by S for the surface) involved in the fit.

It has been early recognized that, in addition to the bulk component (denoted by B), the In 4*d* core level spectrum contains a surface contribution (denoted by S) [34]. Our experimental data is well reproduced using two components with a Voigt profile accounting for the total instrumental (Gaussian) broadening and the lifetime (Lorentzian) broadening with a full width at half maximum (FWHM) of 0.18 and 0.35 eV, respectively. The spin–orbit coupling was set to 0.86 eV. One can also note that the intensity of the surface (S) component is larger for the In-terminated A side than for the B side. The energy shift between the surface and bulk

components is found to be 0.3 eV for the A side, in good agreement with [34], and to be 0.26 eV for the B side [21].

3.2. Bi/InAs(1 1 1): growth modes

From the early stage of the Bi deposition, the LEED pattern of the InAs(1 1 1)A (2 × 2) substrate (figure 1(a)) starts to blur and relatively broad spots showing the formation of Bi(1 1 1) layers appear. For a Bi coverage greater than ≈10 BL, a sharp Bi(1 1 1) (1 × 1) pattern is observed (figure 1(b)).

This is consistent with the fact that the InAs(1 1 1)A surface exhibits a hexagonal pattern of In atoms separated by ≈4.28 Å (figure 1(c)) and the Bi(1 1 1) a honeycomb structure in which the distance between a Bi atom and its second in-plane neighbour is ≈4.55 Å (figure 1(d)). This ≈6% mismatch is not insignificant but small enough to allow the relaxation of the Bi film lattice parameters to their natural values after a deposition equivalent to a few BLs of bismuth and thus the epitaxial growth of Bi(1 1 1) on the InAs(1 1 1)A substrate, for instance in the manner depicted in figure 1(e). For very thin layers (1–2 BL) we do not observe any order by either LEED or ARPES. The substrate In 4*d* PES signal disappears totally for a Bi coverage of ≈10 BL.

The intensity of the Bi 5*d* and In 4*d* PES signals as a function of the Bi evaporation time on InAs(1 1 1)A (not shown) contains a series of linear segments with break points, separated by a common evaporation duration, where a change in slope occurs, which is the well-known signature of a layer-by-layer (Frank–van der Merwe) growth mode. This is consistent with both the LEED patterns (figure 1(b)) and the STM images of these surfaces with terraces having the six-fold symmetry characteristic of the hexagonal arrangement of the Bi atoms on (1 1 1) terraces (figures 1(f) and (g)).

For the InAs(1 1 1)B surface, the intensities of the Bi 5*d* and In 4*d* PES signals as a function of the Bi deposition time also change linearly, but only to the point corresponding to 1 BL coverage. Deviation from the linear behaviour at higher coverage suggests that the Bi growth on the B side of InAs(1 1 1) proceeds via a Stranski–Krastanow mode, contrary to what happens on InAs(1 1 1)A. Indeed the STM images show the presence of such islands on InAs(1 1 1)B [33]. The substrate In 4*d* PES signal remains visible up to deposition equivalent to a coverage of ∼50 BL Bi, above which the Bi three-dimensional islands that build on the surface above 1 BL coalesce.

3.3. Bi/InAs(1 1 1): electronic structure

3.3.1. Bi on InAs(1 1 1)A

Changes in the electronic structure of the Bi/InAs(1 1 1)A interface can be detected at the early stage of the Bi deposition in the In 4*d* PES spectrum (recorded at $h\nu = 40$ eV) (figure 3(a)).

For 0.2 BL coverage the whole spectrum shifts relative to that of the pristine substrate by ≈200 meV towards the low BE side; this shift reaches ≈300 meV for a coverage of ≈1 BL and stabilizes to this value for higher coverage. This shift is accompanied by a change in the overall shape of the In 4*d* spin–orbit doublet. Both effects are due to the progressive disappearance of the surface (S) component of pristine InAs(1 1 1)A (see figure 2). The substrate In 4*d* PES signal disappears totally for a Bi coverage of ≈10 BL.

The spectrum at the bottom of figure 3(a) presents the result of the subtraction of the spectrum for 0.2 BL from that for 2 BL Bi coverage. This difference spectrum is very similar to that corresponding to the surface (S) component in the In 4*d* PES spectrum of pristine InAs(1 1 1)A. This is thus a confirmation of the disappearance of the S component at the early stage of Bi deposition on InAs(1 1 1)A. Note that we did not subtract the In 4*d* PES for 0.2 BL Bi coverage because of the band bending effect induced by the deposition of the first Bi atoms. It is interesting to note that the subtraction reveals a faint structure at ≈17.4 eV BE, i.e. at the BE expected when Bi is chemically bound to In. Such a behaviour is also observed for the Bi/GaAs(1 1 1)A and B interfaces [36, 37], as well as for the Bi/InAs(1 0 0) interface [38, 39].

We now turn to the Bi $5d_{5/2}$ PES signal (figure 3(b)). Its shape converges to that of the bulk Bi signal when the amount of Bi deposited is increased up to ≈10 BL. To shed light on the origin of the changes occurring at low Bi coverage we show at the bottom of figure 3(b) the difference spectrum obtained by subtracting the Bi $5d_{5/2}$ PES spectrum for 15 BL (not shown in the figure as essentially identical to the 10 BL PES spectrum) from that for 0.2 BL Bi coverage, removing in such a way the bulk component. This difference spectrum is made of two components: the one at low BE, of much higher intensity, can be attributed to Bi bound to In and that at high BE to Bi bound to As (see [21]). The latter can be observed despite the InAs(1 1 1)A substrate is In-terminated because some defects due to surface preparation (ion bombardment and annealing) might allow As atoms to be present on the surface. The subtraction clearly indicates that the apparent change in the position of the Bi $5d_{5/2}$ PES upon Bi deposition, namely 0.2 BL, arises from the intensity variation/decrease of the PES component corresponding to the Bi–In bond, similarly to what is observed for the In 4*d* PES signal upon Bi deposition.

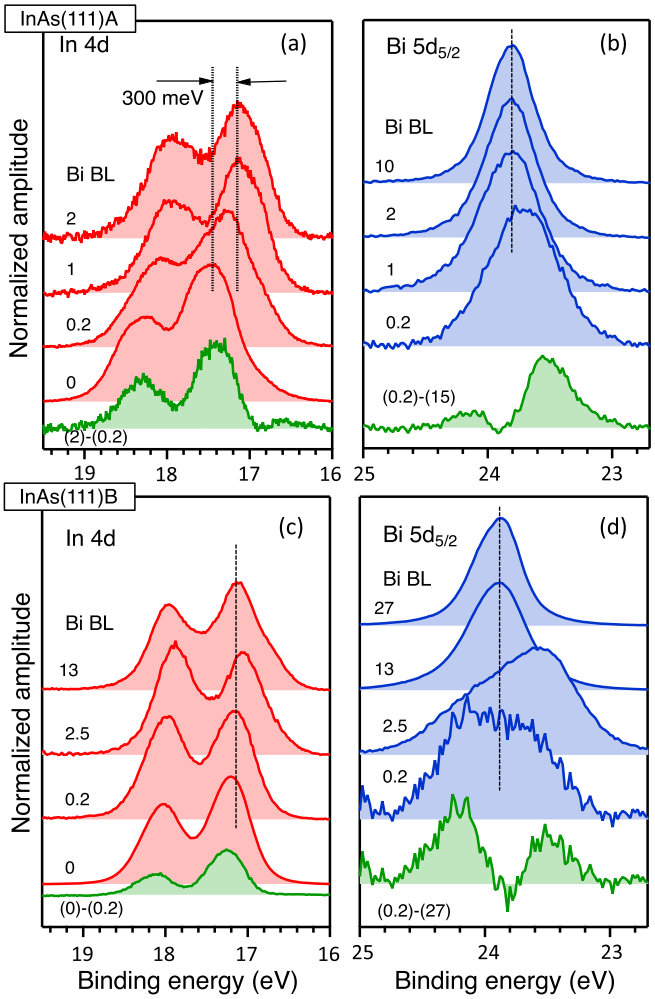

Figure 3. Changes in core level PES spectra upon Bi deposition (in BL) on InAs(1 1 1). InAs(1 1 1)A (top panel): (a) In 4*d* spectra (the difference spectrum between In 4*d* data for 2.0 and 0.2 BL Bi coverage is shown (in green/light grey) at the bottom of the figure); (b) Bi $5d_{5/2}$ spectra (the difference spectrum between Bi $5d_{5/2}$ PES signals for 0.2 and 15 BL Bi coverage is shown (in green/light grey) at the bottom of the figure). InAs(1 1 1)B (bottom panel): (c) In 4*d* spectra (the difference spectrum between In 4*d* data for 0 and 0.2 BL Bi deposition is shown (in green/light grey) at the bottom of the figure); (d) Bi $5d_{5/2}$ spectra (the difference spectrum between Bi $5d_{5/2}$ data for 0.2 and 27 BL Bi deposition is shown (in green/light grey) at the bottom of the figure).

3.3.2. Bi on InAs(1 1 1)B

The evolution of In 4*d* and Bi $5d_{5/2}$ PES spectra on InAs(1 1 1)B is quite different from that on InAs(1 1 1)A (figures 3(c) and (d)). The presence of Bi atoms on the B surface does not induce a shift as observed for InAs(1 1 1)A. This allows a subtraction of the In 4*d* spectrum of the pristine substrate from that corresponding to 0.2 BL Bi deposition (denoted by '(0)–(0.2)' at the bottom of figure 3(c)). Similarly to InAs(1 1 1)A, the surface (S) component disappears at very early stages of Bi deposition. For higher Bi deposition a new low BE feature appears in the spectra.

A better insight of its evolution is shown in figure 4(a) where we plot only difference spectra. The surface component ('(0)-(0.2)' from figure 3(c)) is shown as a reference. Subtracting the In 4*d* spectrum corresponding to 0.2 BL Bi, i.e. containing only the bulk (B) component, from that corresponding to 13 and 27 BL Bi deposits (middle and upper spectrum of figure 4(a), respectively, where only the In $4d_{5/2}$ component is shown) reveals two new structures that can be attributed to Bi–In (higher BE) and In–In (lower BE) components. The presence of such features has been previously suggested [21] but not evidenced. Here, the In–In component clearly appears for higher Bi coverage. We believe that its formation is due to the fact that the Bi–As bond is stronger as compared to the Bi–In one, as deduced from BE shifts [21]. At higher coverage Bi–As bonds are formed and free In atoms are released on the surface. A similar chemical behaviour has been observed when annealing Bi layer on top of an InAs(1 1 1) crystal [24].

The evolution with Bi deposition of the Bi $5d_{5/2}$ PES spectra (figure 3(d)) is in agreement with the above chemical interpretation. As in the case of InAs(111)A, we show at the bottom of figure 3(d) the difference spectrum resulting from the subtraction of the Bi $5d_{5/2}$ PES spectrum for 0.2 BL Bi coverage from that for 13 BL

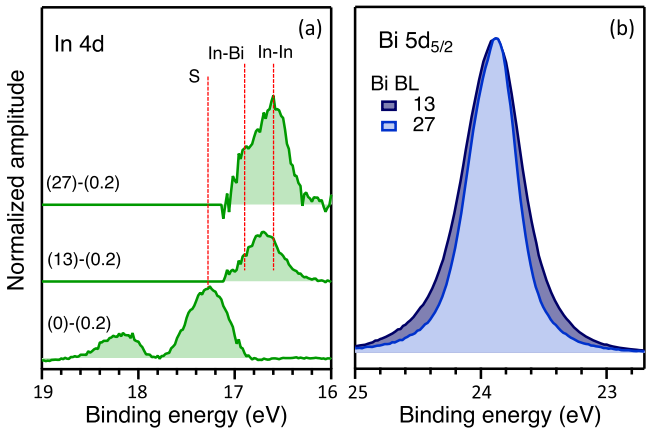

Figure 4. PES difference spectra between Bi-covered (in BL) and pristine InAs(1 1 1)B. (a) In $4d$; (b) Bi $5d_{5/2}$.

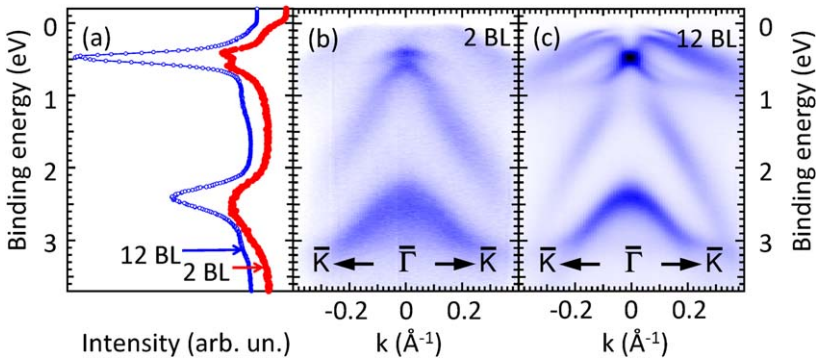

Figure 5. (a) Valence band PES spectra at normal emission of InAs(1 1 1)A covered by 2 and 12 BL Bi. (b) and (c) corresponding ARPES spectra along the $\overline{\Gamma}$–$\overline{\mathrm{K}}$ direction. Spectra were recorded at $h\nu = 20$ eV.

coverage. The final difference spectrum exhibits again two components: the one at high BE has now a larger intensity, which is expected for the As-terminated B side; the presence of the low BE component, attributed to Bi–In bonds, can be justified because the annealing during the sample preparation eliminates preferentially As atoms, leaving In-terminated patches on the surface. This scenario is consistent with further evolution of the Bi $5d_{5/2}$ spectra. For 2.5 BL Bi coverage, as all Bi–As bonds are saturated, the peak related to the Bi–In bonding is dominant. Upon further deposition, the FWHM of the Bi $5d_{5/2}$ feature decreases and reaches that of bulk Bi well above 27 BL (figure 4(b)), when Bi islands coalesce in larger terraces, in clear contrast with what happens in the case of the InAs(1 1 1)A surface. We suggest that the presence of strong Bi–As bonds prevents epitaxial growth at very initial stages of Bi deposition.

Bearing in mind that for such high depositions the In $4d$ PES signal is faint, but still present, this is in line with the formation of 3D Bi islands during the growth. This situation is similar to that encountered when Bi is deposited on GaAs where Bi *bands* have been reported for a 2 BL deposit [36]. Indeed the STM images show the presence of such islands on InAs(1 1 1)B [33].

We deposited as well Bi on InAs surfaces prepared by molecular beam epitaxy (MBE). Interestingly, in spite of the higher quality of these surfaces as compared to those prepared using ion-bombardment–annealing cycles, the Bi growth on the InAs(1 1 1)A is worse. In MBE chambers, it is impossible to suppress instantaneously the As vapour pressure after the InAs substrate growth. So, even MBE prepared In-terminated A face is covered by a fraction of monolayer of As, preventing a good epitaxy. Bi films grown on bombarded/annealed A faces are of much higher quality than those obtained by MBE.

3.4. Bi/InAs(1 1 1)A valence band PES

The ARPES spectra recorded with a photon energy of $h\nu = 20$ eV along the $\overline{\Gamma}$–$\overline{\mathrm{K}}$ direction for Bi coverage of 2 and 12 BL are shown in figure 5. A Bi coverage of 2 BL is sufficient for the ARPES spectrum to show main bands

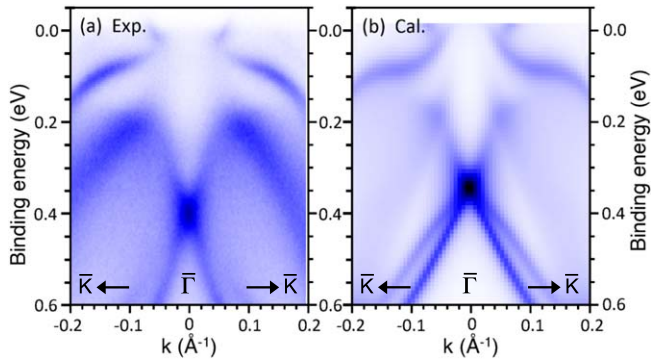

Figure 6. Bi(1 1 1) ARPES spectrum along the $\overline{\Gamma}$–$\overline{\mathrm{K}}$ direction. (a) Experimental data, taken at $h\nu = 20$ eV, for 12 BL Bi(1 1 1) grown on InAs(1 1 1)A. (b) Calculation for $h\nu = 22$ eV.

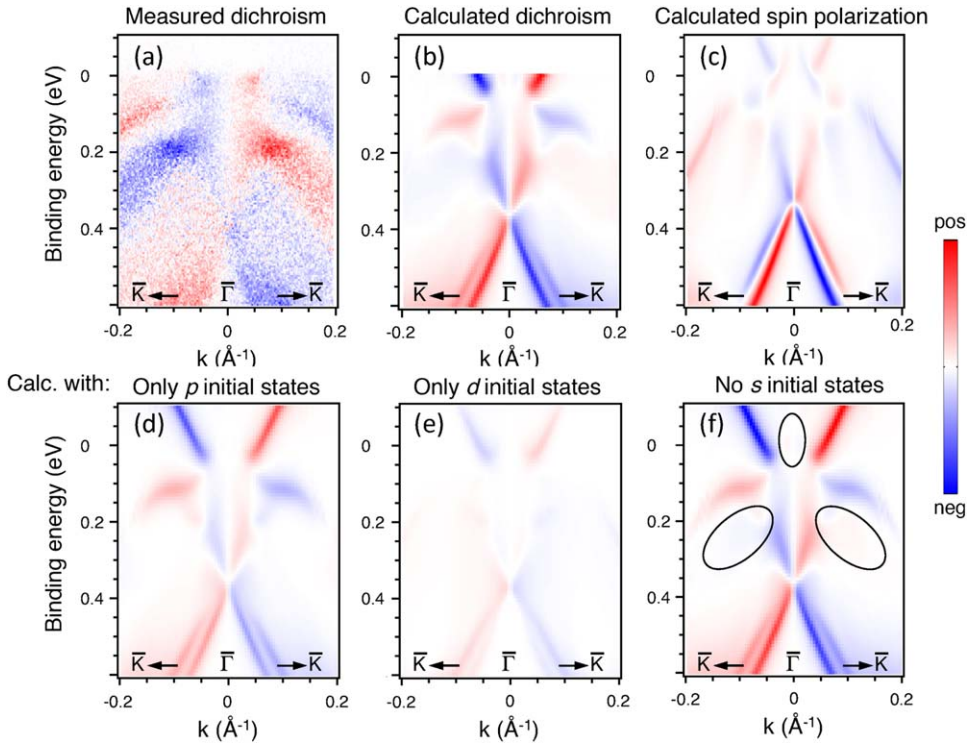

Figure 7. CD-ARPES in the $\overline{\Gamma}$–$\overline{\mathrm{K}}$ direction of Bi(1 1 1). (a) Experiment ($h\nu = 20$ eV) for 20 BL of Bi deposited on InAs(1 1 1)A. (b) Theory ($h\nu = 22$ eV). (c) Calculated spin polarization. (d)–(f) Theoretical analysis of the contribution of the angular momentum in the initial state (respectively, $\ell = 1, 2$ and in absence of $\ell = 0$) to the dichroic response. The blue-red colour scale indicates the sign/strength of the dichroic signal. The ovals indicate the region where bands are lacking only when only either *p* (figure 7(d)) or *d* (figure 7(e)) initial states are considered.

characteristic of bulk Bi (figure 5(b)); in particular Bi states near the Fermi level start to appear in the gap of InAs. We observed that the bands sharpen progressively upon increasing Bi deposition, the whole ARPES spectrum becoming identical to that of bulk Bi (see, e.g. [6]) for ≈12 BL coverage (figure 5(c)). Normal emission spectra in (figure 5(a)), extracted from figures 5(b) and (c), show a strong intensity increase of the surface state resonance at 2 eV BE in the 12 BL deposit (blue curve) that is characteristic for a high quality Bi crystal [6]. This is in complete consistency with the Bi epitaxial growth mode on the A side, as deduced from the analysis of the core level PES spectra (see section 3.2).

The calculated momentum versus energy intensity distribution (see section 2) along the $\overline{\Gamma}$–$\overline{\mathrm{K}}$ direction for a Bi(1 1 1) surface at $h\nu = 22$ eV and the spectrum measured for a 12 BL Bi deposit on InAs(1 1 1)A at $h\nu = 20$ eV are compared in figure 6. The spectra are found to be in good agreement. The misfit in photon

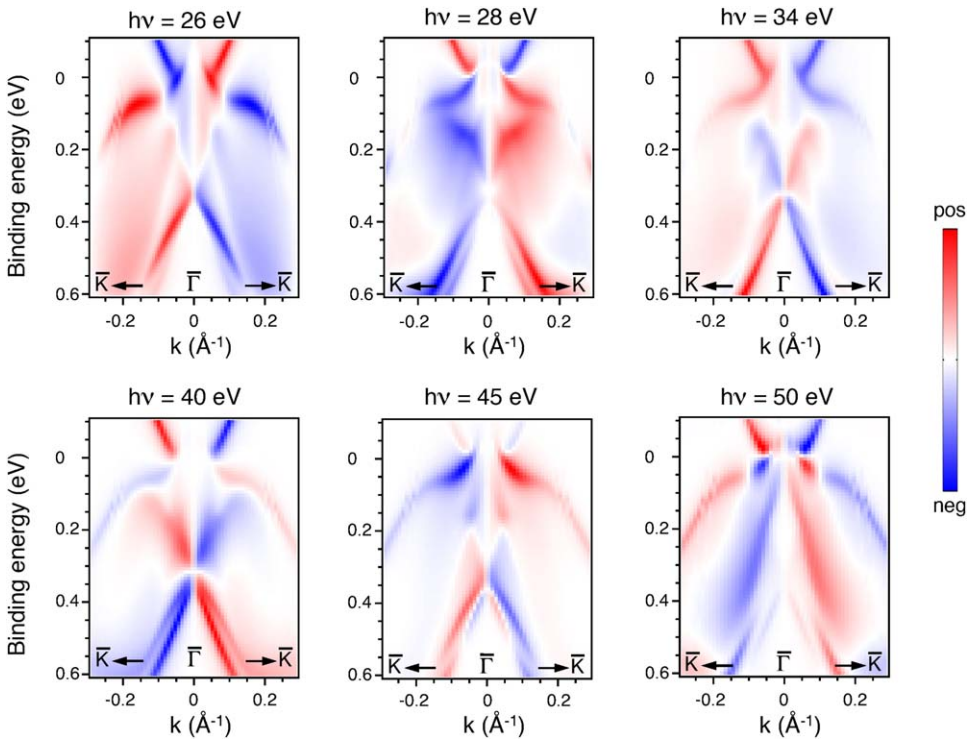

Figure 8. CD-ARPES in the $\overline{\Gamma}$–$\overline{K}$ direction of Bi(1 1 1) calculated for various photon energies. The blue-red colour scale indicates the sign/strength of the dichroic signal.

energy of 2 eV between the measured and calculated final-state bands can be attributed to electron correlation effects beyond the local density approximation in density functional theory [40].

The ARPES spectra were observed to be highly dependent on the helicity of the light used to induce photoemission. This is seen in figure 7(a) which shows the ARPES circular dichroism (CD) in the $\overline{\Gamma}$–$\overline{K}$ direction for a 12 BL Bi deposit on InAs(1 1 1)A obtained from measurements with left/right circularly polarized light at $h\nu = 20$ eV photon energy. The theoretical prediction at $h\nu = 22$ eV (figure 7(b)) reproduces nicely the experimental result. It is to be noted that the measured CD differs significantly from the spin polarization expected from the calculations performed within the same theoretical framework (figure 7(c)). This reinforces the consensus that CD-ARPES is not related directly to the spin texture of the system as already observed in other cases (see, e.g. [41–45]) and cannot replace the much more experimentally demanding spin-resolved ARPES for spin analysis [46, 47] (see [48] for a detailed discussion). Nevertheless CD-ARPES is a useful tool to probe the orbital symmetry. This is illustrated in figures 7(d)–(f) where we show a theoretical analysis of the contribution to the CD of initial states having different angular momenta. Considering either the *p* or *d* initial states (see figures 7(d) and (e), respectively) does not allow to fully recover the whole result (it can be noted that the *p* states contribute much more than the *d* states). The bands in the black ovals in figure 7(f) are reproduced only when *both p* (figure 7(d)) and *d* (figure 7(e)) initial states are considered, i.e. the *s* orbitals are deactivated. This suggests an hybridization of the *p* and *d* states in this (**k**, BE) region.

Another aspect concerning the possible link between CD-ARPES and the spin polarization is the choice of the energy of the incoming photon. This is exemplified in figure 8 where CD-ARPES simulations for the $\overline{\Gamma}$–$\overline{K}$ direction are shown for various photon energies in the 26–50 eV energy range. Sign inversions are theoretically predicted to occur rather regularly in the CD when increasing the photon energy by a few eV steps. This can be attributed to the spin dependence of the relativistic dipole-matrix elements that are strongly sensitive to the final states reached at different photon energies as clearly demonstrated in a comparison between PES experiments and one-step photoemission calculations [42]. Thus, if CD-ARPES can be seen as a quick way to search for spin polarized bands, it will not give a one-to-one mapping of the spin components of the photoemitted electron.

In order to experimentally provide evidence of such sign flips in CD-ARPES in the $\overline{\Gamma}$–$\overline{M}$ direction, we have selected two photon energies, namely 40 and 45 eV. Figure 9 shows the comparison between measurements and theoretically expected results. Various sign changes are seen, depending on the spectral region (some examples are indicated by black arrows in figure 9), even though the calculations are only in limited agreement with experiment. It is also to be underlined that, for a given photon energy, a change in the crystallographic direction has a dramatic influence on the CD-ARPES signal observed.

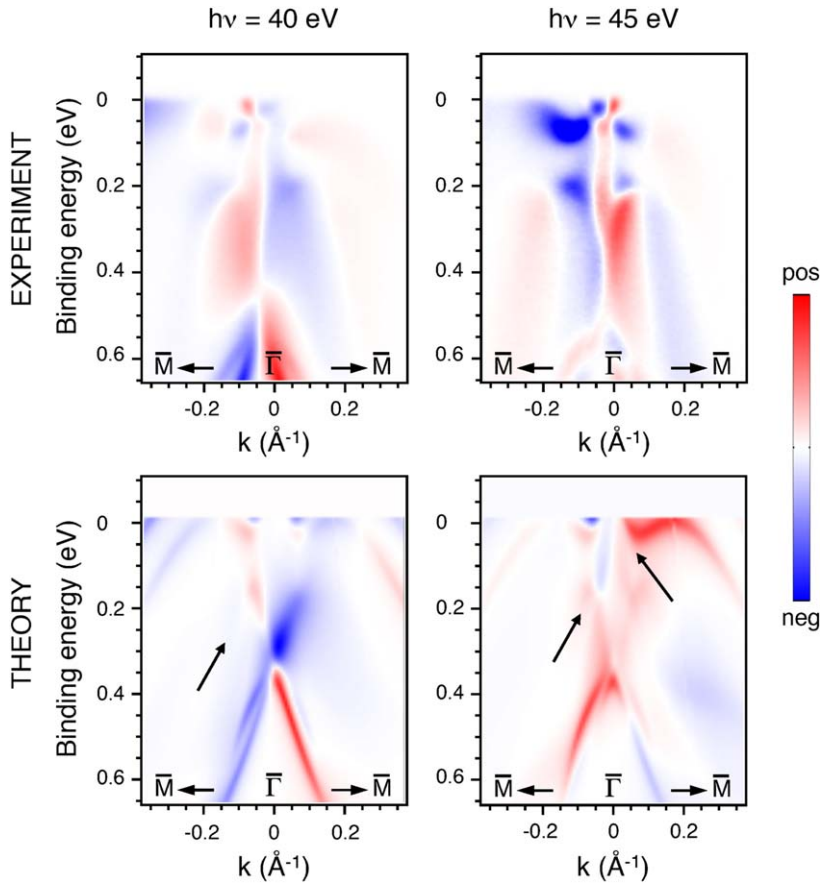

Figure 9. CD-ARPES in the $\overline{\Gamma}$–$\overline{\mathrm{M}}$ direction at 40 and 45 eV photon energy: comparison between experiment (top) and theory (bottom). Some sign inversions observed in both experiment and theory are indicated by black arrows. The blue-red colour scale indicates the sign/strength of the dichroic signal.

4. Conclusions

We have shown that the growth of Bi thin films on InAs(1 1 1) substrates present distinctive behaviours depending on the atomic surface termination. The analysis of Bi and In core-level photoelectron spectra indicates that Bi growth is epitaxial on the InAs(1 1 1)A surface, contrary to that on the InAs(1 1 1)B surface. Deposition of $\gtrapprox$10 BL of Bi on InAs(1 1 1)A results in a Bi monocrystal of very high quality as attested by comparison of valence band photoemission data with previous results obtained on the bulk material. Our results are also supported by state-of-the-art theoretical simulation of the photoemission process. A detailed comparison between theory and experiment on the circular dichroism in photoemission suggests a *p*–*d* hybridization of the valence states in the vicinity of the $\overline{\Gamma}$ point. Finally the strong influence of the final states on the dichroism in photoemission for this system is revealed, giving an illustration that dichroism in photoemission has to be used with care for probing the spin texture of topological systems.

Acknowledgments

The research leading to these results has received funding from the European Community's Seventh Framework Programme (FP7/2007–2013) under grant agreement No. 312284. JB and HE acknowledge financial support by the Deutsche Forschungsgemeinschaft SPP1666 priority program (Grants No. EB144/26 and EB154/32). JM and LN would like to thank the Computational and Experimental Design of Advanced Materials with New Functionalities (CZ.02.1.01/0.0/0.0/15_003/0000358) co-funded by the European Regional Development Fund as part of the Ministry of Education, Youth and Sports of Czech Republic. OH, KH and MCR acknowledge funding from the 'Investment for the Future' programme of the Agence Nationale de la Recherche (contract No 11-EQPX-0034-PATRIMEX).

ORCID iDs

K Hricovini https://orcid.org/0000-0002-7541-1942

References

[1] Hasan M Z and Kane C L 2010 *Rev. Mod. Phys.* **82** 3045–67
[2] Qi X-L and Zhang S-C 2011 *Rev. Mod. Phys.* **83** 1057–110
[3] Ando Y 2013 *J. Phys. Soc. Jpn.* **82** 102001
[4] Hasan M Z, Xu S Y and Bian G 2015 *Phys. Scr.* **T2015** 014001
[5] Rashba E I 1960 *Sov. Phys. Solid State* **2** 1109–22
Rashba E I 1960 *Fiz. Tverd. Tela (Leningrad)* **2** 1224–38
[6] Hofmann Ph 2006 *Prog. Surf. Sci.* **81** 191–245
[7] Takayama A, Sato T, Souma S and Takahashi T 2011 *Phys. Rev. Lett.* **106** 166401
[8] Takayama A, Sato T, Souma S, Oguchi T and Takahashi T 2012 *Nano Lett.* **12** 1776–9
[9] Huang H, Wong S L, Wang Y, Sun J-T, Gao X and Wee A T S 2014 *J. Phys. Chem.* C **118** 24995–9
[10] Kowalczyk P J, Mahapatra O, McCarthy D N, Kozlowski W, Klusek Z and Brown S A 2011 *Surf. Sci.* **605** 659–67
[11] Gao C-L, Qian D, Liu C-H, Jia J-F and Liu F 2013 *Chin. Phys.* B **22** 67304
[12] Drozdov I K, Alexandradinata A, Jeon S, Nadj-Perge S, Ji H, Cava R J, Bernevig A B and Yazdani A 2014 *Nat. Phys.* **10** 664–9
[13] Takayama A, Sato T, Souma S, Oguchi T and Takahashi T 2015 *Phys. Rev. Lett.* **114** 066402
[14] Hricovini K, Richter M C, Heckmann O, Nicolaï L, Mariot J-M and Minár J 2019 *J. Phys.: Condens. Matter* **31** 283001
[15] Murakami S 2006 *Phys. Rev. Lett.* **97** 236805
[16] Wada M, Murakami S, Freimuth F and Bihlmayer G 2011 *Phys. Rev.* B **83** 121310
[17] Liu Z, Liu C-X, Wu Y-S, Duan W-H, Liu F and Wu J 2011 *Phys. Rev. Lett.* **107** 136805
[18] Huang Z-Q, Chuang F-C, Hsu C-H, Liu Y-T, Chang H-R, Lin H and Bansil A 2013 *Phys. Rev.* B **88** 165301
[19] Hsu C H, Huang Z Q, Chuang F C, Kuo C C, Liu Y T, Lin H and Bansil A 2015 *New J. Phys.* **17** 025005
[20] Reis F, Li G, Dudy L, Bauernfeind M, Glass S, Hanke W, Thomale R, Schäfer J and Claessen R 2017 *Science* **357** 287–90
[21] Szamota-Leandersson K, Leandersson M, Göthelid M and Karlsson U O 2011 *Surf. Sci.* **605** 12–7
[22] Panaccione G *et al* 2009 *Rev. Sci. Instrum.* **80** 043105
[23] Balasubramanian T *et al* 2010 *AIP Conf. Proc.* **1234** 661
[24] Richter M C *et al* 2016 *Surf. Sci.* **651** 147–53
[25] Ebert H, Ködderitzsch D and Minár J 2011 *Rep. Prog. Phys.* **74** 096501
[26] Braun J 1996 *Rep. Prog. Phys.* **59** 1267–338
[27] Braun J, Minár J and Ebert H 2018 *Phys. Rep.* **740** 1–34
[28] Rundgren J and Malmström G 1977 *J. Phys. C: Solid State Phys.* **10** 4671–87
[29] Mönig H, Sun J, Koroteev Yu M, Bihlmayer G, Wells J, Chulkov E V, Pohl K and Hofmann Ph 2005 *Phys. Rev.* B **72** 085410
[30] Mankefors S, Nilsson P O and Kanski J 1999 *Surf. Sci.* **443** L1049–54
[31] Taguchi A 2005 *J. Cryst. Growth* **278** 468–72
[32] Taguchi A and Kanisawa K 2006 *Appl. Surf. Sci.* **252** 5263–6
[33] Hilner E, Lundgren E and Mikkelsen A 2010 *Surf. Sci.* **604** 354–60
[34] Andersson C B M, Olsson L Ö, Håkansson M C, Ilver L, Karlsson U O and Kanski J 1994 *J. Phys.* IV **4** 209–12
[35] Szamota-Leandersson K, Göthelid M, Tjernberg O and Karlsson U O 2003 *Appl. Surf. Sci.* **212–213** 589–94
[36] McGinley C, Cafolla A A, Murphy B, Teehan D and Moriarty P 1999 *Appl. Surf. Sci.* **152** 169–76
[37] McGinley C, Cafolla A A, McLoughlin E, Murphy B, Teehan D, Moriarty P and Woolf D A 2000 *Appl. Surf. Sci.* **158** 292–300
[38] Szamota-Leandersson K, Leandersson M, Palmgren P, Göthelid M and Karlsson U O 2009 *Surf. Sci.* **603** 190–6
[39] Ahola-Tuomi M, Punkkinen M P J, Laukkanen P, Kuzmin M, Lång J, Schulte K, Pietzsch A, Perälä R E, Räsänen N and Väyrynen I J 2011 *Phys. Rev.* B **83** 245401
[40] Braun J 2001 New developments in UPS and XPS from ferromagnetic materials *Band-Ferromagnetism* (*Lecture Notes in Physics* Vol 580) ed K Baberschke, W Nolting and M Donath (Berlin: Springer) pp 341–55
[41] Kim B *et al* 2012 *Phys. Rev.* B **85** 195402
[42] Scholz M R *et al* 2013 *Phys. Rev. Lett.* **110** 216801
[43] Vidal F, Eddrief M, Rache Salles B, Vobornik I, Velez-Fort E, Panaccione G and Marangolo M 2013 *Phys. Rev.* B **88** 241410
[44] Sánchez-Barriga J *et al* 2014 *Phys. Rev.* X **4** 011046
[45] Xu C-Z, Liu Y, Yukawa R, Zhang L-X, Matsuda I, Miller T and Chiang T-C 2015 *Phys. Rev. Lett.* **115** 016801
[46] Wang Y H, Hsieh D, Pilon D, Fu L, Gardner D R, Lee Y S and Gedik N 2011 *Phys. Rev. Lett.* **107** 207602
[47] Wang Y and Gedik N 2013 *Phys. Status Solidi RRL* **7** 64
[48] Dil J H 2019 *Electron. Struct.* **1** 023001